Journal of Molecular Graphics and Modelling 59 (2015) 1–13

Contents lists available at ScienceDirect

Journal of Molecular Graphics and Modelling

journal homepage: www.elsevier.com/locate/JMGM

Interactions between Bcl-xl and its inhibitors: Insights into ligand design from molecular dynamics simulation

Prerna Priya, Atanu Maity, Sarmistha Majumdar, Shubhra Ghosh Dastidar*

Bioinformatics Centre, Bose Institute, P-1/12 C.I.T. Scheme VII M, Kolkata 700054, India

ARTICLE INFO

Article history:
Accepted 25 February 2015
Available online 6 March 2015

Keywords:
Bcl-xl
MD simulations
Free energy
MM-GBSA
Ligand
Interfacial water

ABSTRACT

The Bcl-xl protein is a potential drug target for cancer, and it has a relatively flat and flexible binding pocket. ABT263 is one of the most promising molecules that inhibit Bcl-xl, and it was developed from its precursor ABT737 with suitable substitutions. However, the structural and mechanistic implications of those changes have not yet been reported. Molecular dynamics simulation has revealed that the conformational microstates of the complex of Bcl-xl and ABT263 shows heterogeneity at the binding interface with Bcl-xl in contrast to the precise interactions witnessed in case of ABT737. This occurs because not all the functional groups of ABT263 are able to anchor into the binding pocket simultaneously at the time of complexation; leaving at least one group weakly associated every time. The insight into the mechanism shows that, in spite of such mutual exclusivity, the resultant effect becomes beneficial, i.e., becomes more effective than ABT737. Going against the traditional belief, the calculations also confirm that there is no benefit of reshaping the highly flexible binding pocket to allow the ligand to be comfortably accommodated and avoid conflicting orientations of the functional groups, as the destabilization becomes active from other sources. These structural clues and *in-silico* tests suggest possible avenues for improving the binding affinity of ABT263 through further *in-vitro* and *in-vivo* tests.

1. Introduction

Apoptosis is a homeostatic mechanism that programs the death of damaged and unwanted cells [1,2]. Defects in this mechanism can lead to diseases like cancer. Apoptosis has extrinsic and intrinsic pathways [3–5], and Bcl-2 family proteins are known to be key regulators of the intrinsic route [6–8]. Bcl-2 family proteins contain multiple homologous domains, and these proteins are classified in two different subgroups: pro- and anti-apoptotic. A third group also exists, named 'BH3-only', which is a small peptide and functions as a sensor. Pro-apoptotic proteins oligomerize and generate pores in the mitochondrial membrane, facilitating the release of apoptotic factors (e.g., cytochrome *C* and Sma c into the cytosol) [2,9,10]. Anti-apoptotic proteins bind to the pro-apoptotic proteins and inhibit their oligomerization to further block apoptosis [11–13]. Healthy cells maintain the balance between these two classes of proteins, whereas over-expression of anti-apoptotic proteins is reported in many cancerous cells [14]. Bcl-xl is an anti-apoptotic member of the Bcl-2 family and over-expressions of this protein are reported in many cancerous cells (Fig. 1a) [15–19]. Therefore, Bcl-xl is considered as a potential drug target for arresting cancerous growth. Despite being such a lucrative drug target, Bcl-xl is considered to be undruggable due to its flat, extended contact surface (i.e., lacking a well-defined binding groove suitable for tight occupation by a small molecule) and its intracellular localization [20,21]. However, the three-dimensional structures of Bcl-xl (and other homologs, e.g. Bcl2) complexed with pro-apoptotic proteins suggested that the anti-apoptotic proteins consist four hydrophobic groove (length ~20 Å), P1 to P4 that serves as a binding site for BH3-only proteins, can act as a drug target. The binding grooves P1–4 refer to the position of anchoring of four conserved residues (h1–4) of BH3 peptides, all of which appear on the same face of the helix, which has been shown in the Fig. 1b [22–25]. In 2005, Oltersdorf et al. designed a new molecule, ABT737 (Fig. 1c), to target these grooves based on 'structure-activity relationships' (SARs) that complemented the

Abbreviations: ΔG, binding free energy; Δ*E*, change in enthalpy; $\Delta\Delta E_{Tot}$, change in enthalpy in presence of selected explicit water–change in enthalpy in complete implicit environment; ABNR, adopted basis Newton Raphson; Bcl-2, B-cell lymphoma-2; Bcl-xl, B-cell lymphoma extra large; CMAP, cross term map; CHARMM, chemistry at Harvard molecular mechanics; CGENFF, CHARMM generalized force-field; GBSA, generalized Born and surface area; GBMV, generalized Born model utilizing molecular volume; ITC, isothermal titration calorimetry; MD, molecular dynamics; MM, molecular mechanics; NMR, nuclear magnetic resonance; PBSA, Poisson–Boltzmann surface area; PDB, protein data bank; PME, particle mesh Ewald; SA, surface area; SAR, structure activity relationship.

* Corresponding author. Tel.: +91 33 2569 3332; fax: +91 33 2355 3886.
E-mail addresses: sgd@jcbose.ac.in, sgducd@gmail.com (S. Ghosh Dastidar).

http://dx.doi.org/10.1016/j.jmgm.2015.02.005
1093-3263/

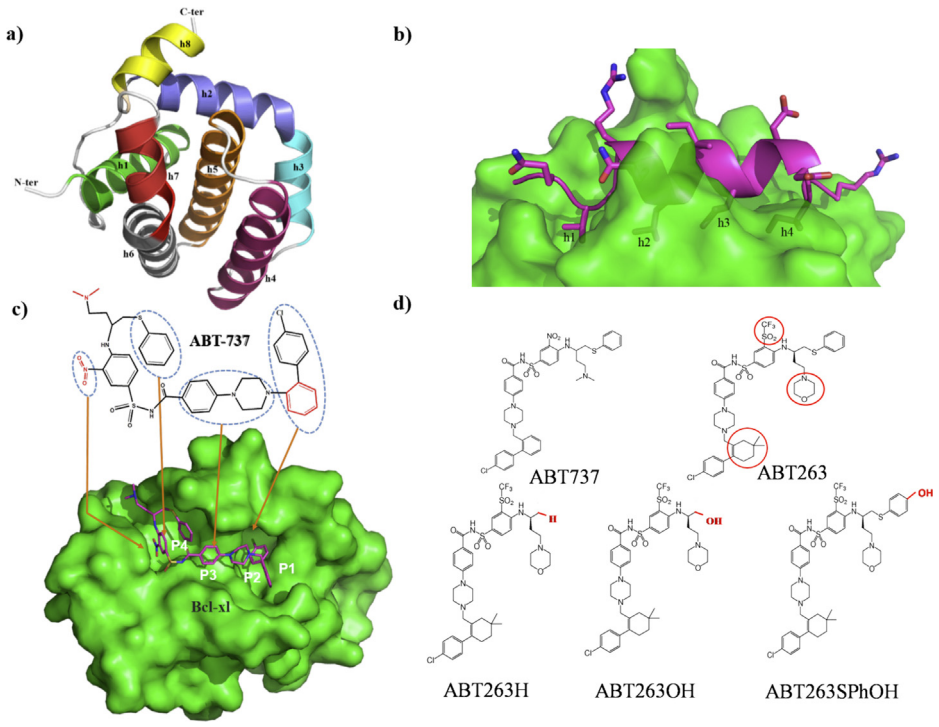

Fig. 1. (a) Cartoon representation of Bcl-xl obtained from PDB code 2YXJ; helices are represented in different colors. (b) The side view of the pockets of Bcl-xl (obtained from PDB code 1BXL) showing the importance of these pockets that enables the anchoring of four conserved residues (h1, h2, h3 and h4) of pro-apoptotic protein, which determines an important part of the Bcl2 family of proteins (c) Binding mode of ABT737 with Bcl-xl as observed from the 2YXJ, showing the Bcl-xl in surface (green) representation. The nomenclature of four pockets (P1–4) refers to the positions where the conserved residues (h1–4) bind otherwise (see text). ABT737 is represented by sticks and colored atoms (C: magenta, N: blue, O: red, S: yellow), (d) Structure of ABT737, ABT263 other derivatives reported in this work. (For interpretation of the references to color in this figure legend, the reader is referred to the web version of this article.)

NMR experiments [26]. Although, later it appeared that ABT737 does not occupy P1 and thus gets characterized more as a functional mimic than a structural mimic of BH3, as mentioned earlier by Lee et al. [27]. The success in designing ABT737 was an achievement in drug discovery for an apparently undruggable target [20,28]. However, low solubility led ABT737 to fail in pre-clinical trials. Later, in 2006, the new inhibitor ABT263 was developed by replacing several functional groups of ABT737. As a result, the molecule becomes soluble as well as orally bio-available (Fig. 1d and Supporting information Fig. S1) with higher probability to bind [29–31]. However, for such an important lead compound, structural insights are not yet available from the experiments, and there are no data available on the consequences of the functional group substitutions on the binding mechanism. In this report the complex of Bcl-xl and ABT263 has been modeled in two different ways: (i) using Bcl-xl + ABT737 complex as template, (ii) using Bcl2 + ABT263 complex as templates, followed by molecular dynamics (MD) based refinement and conformational sampling. There are previous reports on the MD based studies on the interaction of Bcl-xl with their pro-apoptotic partners and inhibitors [32–34]. Lama et al. have provided critical insight into the behaviour of the hydrophobic grooves (P1–4) that enables the receptor to accommodate diverse set of BH3 ligands [34]. In that direction, this present report takes the investigation forward to test the mechanism of binding of two different ligands to that flexible receptor. Although biochemical experiments have revealed better performance of ABT263 [29], the thermodynamic measurements (ITC data or binding constant) on the binding of Bcl-xl with ABT737 and ABT263 are not yet available in the literature. There is only limited available information to figure out their binding affinities [30,31]. In one report, EC50 for Bcl-xl and ABT737 binding is 78.7 nM whereas in another report K_i for ABT737 and ABT263 are found to be less than 0.5 nM. The data refer to different experimental procedures and also not a direct calorimetric measurement of binding. Overall, the data on these ligands imply that ABT263 binds to Bcl-xl more promisingly than ABT737 to reflect their biological action; however, their free energy differences have not yet been directly quantified. Nevertheless, it is important to understand the micro-details of the interactions of these ligands with Bcl-xl, such as how they are similar, how much they differ, and whether the substitutions have any impact on the mechanism of binding. The motivation of the study is not to estimate the binding free energy for comparisons between the two ligands, as the experimental benchmark is not readily available, but certainly the computed energies of binding would serve as an important tool to probe the mechanism correlating the structural consequences. In particular, the changes in the contributions of the energy components (e.g., van der Waals, polar, non-polar) would help to understand the different layers of complexity of the mechanism, which is not yet easy to achieve from experiments.

2. Methods

2.1. Construction of structural models

2.1.1. Bcl-xl + ABT737 complex (Bxl737)

The crystal structure of ABT737 complexed with Bcl-xl was obtained from the Protein Data Bank (PDB) with the accession code 2YXJ (resolution 2.20 Å) [27]. Chain B was extracted with the associated ligand and crystallographic water. The system was solvated with explicit water and was set for MD simulation as described below. The uncomplexed Bcl-xl (Bxl) was modeled by removing the ligand from the complex.

2.1.2. Bcl-xl + ABT263 complex (Bxl263)

For the Bcl-xl–ABT263 complex, the conformation of Bxl737 was used as a template. In the template, the ligand (ABT737) was

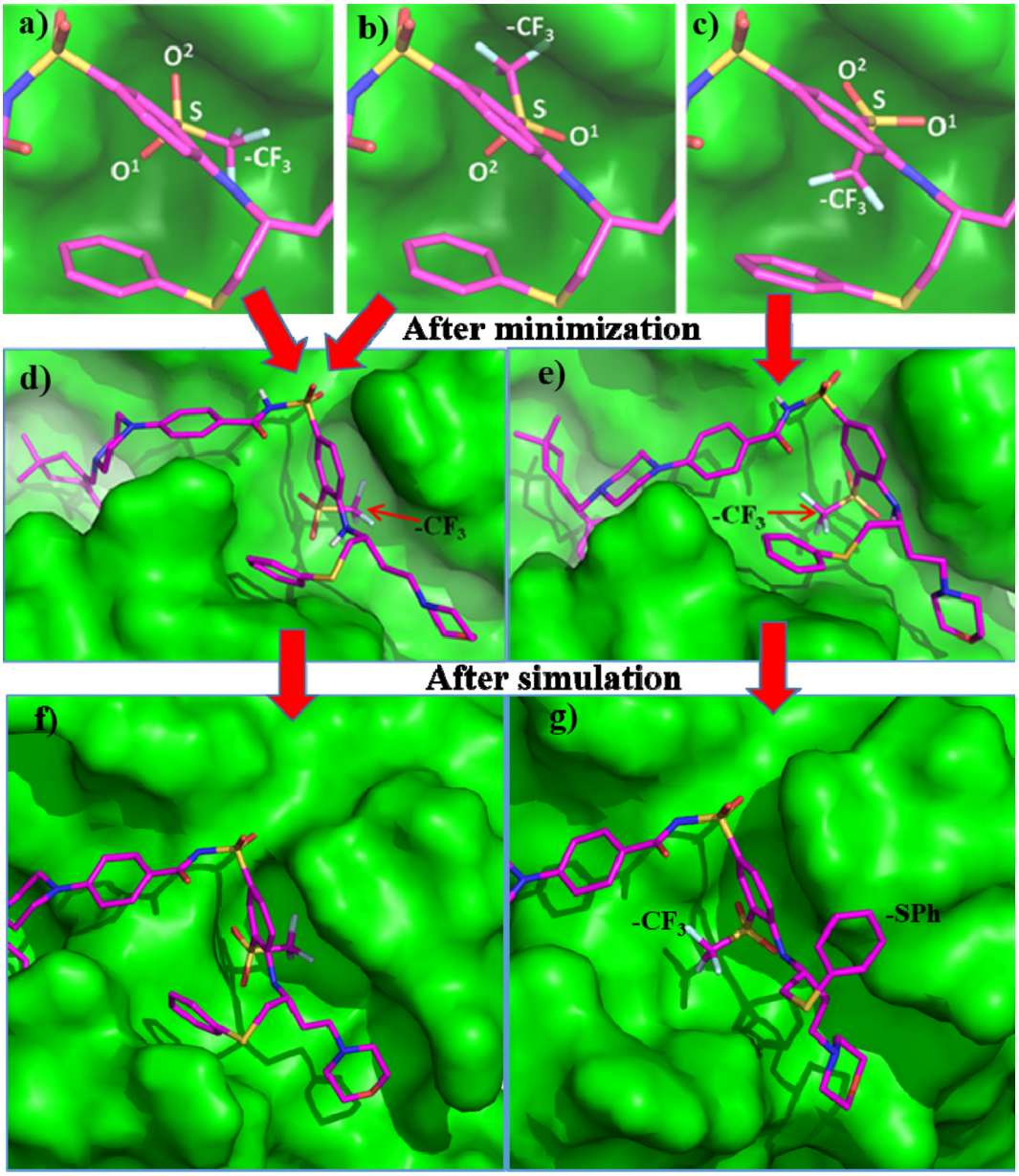

Fig. 2. (a)–(c) Three different orientations of the SO_2CF_3 group of ABT263 (in stick); the surface of Bcl-xl appears with green color. After energy minimization, two of them (a and b) converge into the orientation represented by (d); and (c) minimizes to the structure shown in (e). The conformations (d) and (e) serves as the starting points of two separate simulations, which yielded conformations as shown in (f) and (g), respectively. (For interpretation of the references to color in this figure legend, the reader is referred to the web version of this article.)

suitably edited using Discovery studio 3.5 [36] to generate the desired model of the complex (Fig. 2). The structural arrangement of the skeleton primarily places the SO_2CF_3 inside the P4 pocket. Due to rotation of the bond between 'S' atom and 'C' of the aromatic ring, the SO_2CF_3 group can have three possible orientations. Each conformer differed by a 120° rotation and was considered separately for each simulation. Although we started from three such different models, two of the original distinct orientations converged to a similar orientation due to steric hindrance with the protein (Fig. 2a–e).

2.1.3. Orientation of Y195

The PDB structure (4LVT) of Bcl2 + ABT263 complex shows a different conformation of Y199 of Bcl2 (equivalent to Y195 of Bcl-xl) that creates space for anchoring of the ligand (Fig. S2). [35]. Bcl-2 being homologous to Bcl-xl [27,35], suggested the investigation of the tyrosine orientation to modulate the binding. Therefore a separate model of the complex was prepared by rotating side chain of Y195 (similar to 2YXJ) similar to 4LVT. To complement this, two different orientations of $-CF_3$ (of ABT263) was modeled in separate simulations (i) pointing toward the periphery of the pocket ($BxlY^{rot}$cf3-p, Fig. 3a), (ii) pointing toward the center of the pocket ($BxlY^{rot}$cf3-c, Fig. 3b).

2.1.4. Homology modeling of Bcl-xl + 263(ModBxl263) and uncomplexed Bcl-xl (ModBxl)

The ABT263 binding face of Bcl-xl was modeled also separately using the Bcl2-ABT263 complex (PDB ID 4LVT) as a template; to test the alternative arrangements of the side chains, including Y195. Similarly the uncomplex Bcl-xl was also modeled. The Modeling was performed using EasyModeller 4.0 [37].

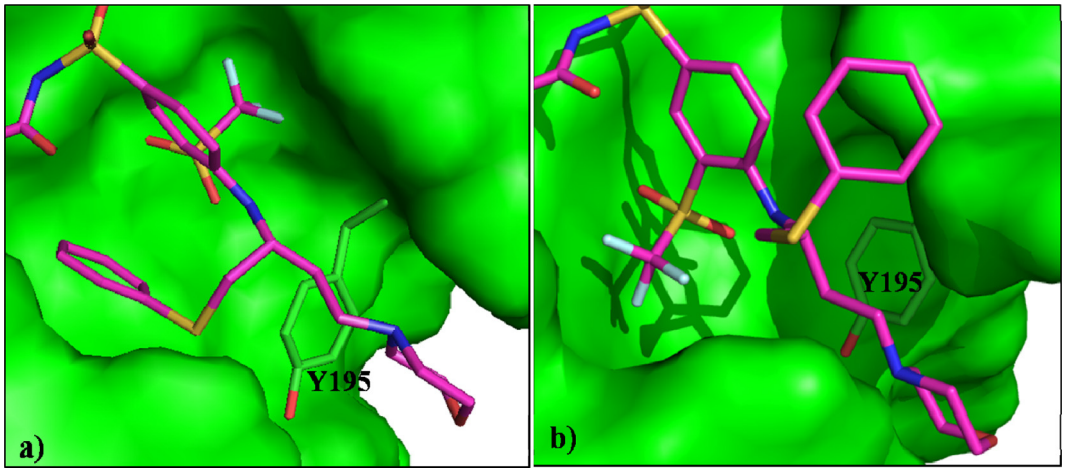

Fig. 3. Two different starting point of two separate simulations after modeling the side chain orientation of Y195 to follow the orientation of its equivalent residue (Y199) in Bcl2 + ABT263 complex as witnessed in 4LVT. The structures shown in (a) and (b) differ in the orientations of —SO_2CF_3 and —SPh extracted from the last frame of the $Bxl263^{in}$ and $Bxl263^{out}$, respectively.

2.1.5. *Bcl2 + ABT263 (Bcl263) complex and uncompelxed Bcl2 (Bcl2)*

The structure of Bcl2 with ABT-263 is taken from Potein Data Bank (4LVT) and the simulation of both apo and holo form was performed.

2.1.6. *Complexes of ABT263 derivatives*

The derivatives of ABT263 were prepared (Supporting information Table S1) by suitable additions and/or substitutions.

The protein–ligand interactions plots were prepared using LIGPLOT$^+$ v. 1.4.5 [38].

2.2. *Molecular dynamics (MD) simulation*

The systems were created using the CHARMM-GUI web-server [39]. Eighteen systems were prepared as listed in Supporting information Table 1. Each of them was solvated in a cubic TIP3P water box by maintaining a minimum 9 Å thickness of the water layer everywhere and a 0.15 M salt concentration by adding the appropriate number of potassium and chloride ions [40]. Energy minimization was performed using Adopted Basis Newton–Raphson methods followed by Conjugate Gradient methods. Molecular Dynamics Simulation was performed using the NAMD package [41]. CHARMM22 force-field [42] with CMAP corrections [43] were used for the protein, solvent, and Ions; CHARMM Generalized Force-Field (CGENFF) [44] was used for the ligands. The systems were heated to 300 K during 10 ps of the simulation and then equilibrated for 15 ps. Then, the production run was performed under NPT conditions, maintaining 300 K temperature and 1 atmosphere pressure using a Nose–Hoover thermostat/barostat. The integration time step was set to 1.0 fs, and the coordinates were saved at 1 ps intervals. Short-ranged non-bonded interactions were truncated at 12 Å, and the particle mesh Ewald (PME) [45] method was used to calculate the long-range electrostatic interactions. Each system was primarily run for 80 ns, whereas some of their derivatives were run for a shorter length of time, and altogether, 1120 ns sampling was achieved. Details of the simulated systems and the duration of the simulation are listed in Supporting information Table S1. Movies and figures were prepared using VMD [46] and Pymol [47].

2.3. *Binding free energy calculations*

The standard free energy of binding ($\Delta G^{o}_{Binding}$) was calculated using the MM-GBSA (Molecular Mechanics with Generalized Born and Surface Area) protocol. MM-GBSA has its foundation in the fundamentals of statistical thermodynamics, whose details are available in the literature [48–50]. In practice, the simulations of the uncomplexed and the complexed states are performed using explicit water to get the conformational microstates of the solute, and then the free energy of solvation of these conformations are estimated using an implicit environment after removal of explicit water molecules. More details are available in the Supporting information (SI). The Poisson–Boltzmann (PB) combined with solvent accessibility (SA), or PBSA, method is well accepted as a benchmark for calculating solvation energy [51–53]. However, the calculation is computationally demanding and is often confounded by the computing capacity. Additionally, the derivatives, i.e., forces, are poorly defined unless one changes the definition to the molecular volume. Computationally less expensive methods are favored to analyze thousands of snapshots. The generalized born combined with solvent accessibility (GBSA) method is a modified and faster derivative

Table 1
Binding energy of different ligands with Bcl-xl and Bcl2.

Components of energy	$\Delta_{Binding}$ (kcal/mol)									
	ABT737	$ABT263^{in}$	$ABT263^{out}$	ABT263H	ABT263OH	ABT263SPhOH	$Bxl263Y^{rot}cf3\text{-}p$	$Bxl263Y^{rot}cf3\text{-}c$	ModBxl263	Bcl2-263
ΔE_{ELEC}	93.3	−172.7	−101.6	−23.4	−31.3	−21.3	−18.0	77.1	52.1	6.9
ΔE_{VDW}	−78.4	−101.1	−70.3	−83.5	−81.1	−84.3	−93.3	−81.9	−73.2	−48.9
ΔE_{INTER}	2.3	−4.6	−14.0	−5.3	−8.3	−24.7	−5.7	0.5	0.1	−19.5
$\Delta E_{GB(Polar)}$	−66.7	216.7	115.0	76.6	59.3	47.9	50.5	−37.5	−40.7	16.8
$\Delta E_{GB(Nonpolar)}$	−6.1	−8.3	−7.1	−6.8	−7.5	−8.2	−8.8	−7.0	−6.8	−5.9
$\Delta E_{GB(Polar)+Elec}$	26.6	44.0	13.4	53.2	28.0	26.6	32.5	39.6	11.4	23.6
$\Delta E_{MM\ (TOT.)}$	−55.6	−70.0	−78.0	−42.4	−68.9	−90.6	−75.3	−48.8	−68.5	−50.6
$-T\Delta S$	+30.4	+43.6	+33.2	+26.0	+30.1	+34.3	+40.4	+33.2	+25.2	+24.2
ΔG	−25.2	−26.4	−44.8	−16.4	−38.8	−56.3	−34.9	−15.6	−43.3	−26.4

of PBSA that is widely used for such calculations [54–57]. Using the MM-GBSA method, relative binding affinity has often been reproduced with good accuracy and considerable less computational effort [57–59]. The GBSA method has a parametric dependence on a supplied set of GB atomic radii, which depend on the force-field used, in contrast to the atomic radii used in PBSA [60,61]. The Generalized born model utilizing molecular volume (GBMV) method is an advanced version of GB that computes Born radii very accurately, often with greater than 99% accuracy, using CHARMM force-field [62]. However, it is slower than other methods, such as GBORN, ACE and GBSW, but faster than MM-PBSA. In this work, GBMV [61–63] was used. The entropic contribution to the binding was estimated using the normal mode analysis; the combination of MM-GBSA and NMA is widely accepted and suitable for our purpose [59,64]. The MMGBSA calculations were performed over the 2000 snapshots taken during the last 20 ns of each system, allowing sufficient time to optimize their interactions in each complex. Normal modes were performed over 200 frames separated by 10 ps over the last 20 ns in each case.

The role of interfacial water in binding of the ligand with a protein is often argued to be an important issue. However, its impact is not reflected on the binding affinity in the MM-GBSA calculation unless those important water molecules are included explicitly in the calculations [65,66]. To test the significance of the presence of such important 'constructing' water molecules, a separate set of calculations for $\Delta E_{\text{binding}}$ was performed on a selected system using the MM-GBSA method that considers explicit water molecules within a cut off of 3 Å from both the ligand and protein. The water molecules were selected at each timeframe. The structures of the uncomplexed states were prepared by splitting the trajectory of the complex into the ligand and receptor because it is difficult to select exactly the same number of water molecules for both the complexed and uncomplexed states from separate trajectories. The calculation was repeated with and without water molecules to note the difference in $\Delta E_{\text{binding}}$ due to the presence of explicit water molecules.

3. Results

The binding mechanisms of flexible biomolecules generally proceed through mutual induction of conformational changes. To study the complexation of the flexible protein Bcl-xl with its ligand, it is essential to simulate the complexed and uncomplexed states separately. A popular alternative method is to simulate the complex and then split the structures into the ligand and receptor to save computing time. However, this method often overlooks the effect of conformational adjustments on the binding energy, although such reports are available for the Bcl-2 family in the literature [22,33,67]. Bcl-xl contains four hydrophobic pockets named P1, P2, P3 and P4 that allow the binding of four conserved hydrophobic residues (h1–h4) of pro-apoptotic proteins (Fig. 1b and c). As the surface of the protein is flexible, the shape of binding groove changes to complement the ligand.

3.1.1. Uncomplexed Bcl-xl

When Bcl-xl was simulated after removing ligand from the complex obtained from PDB, the amino acids around the binding pocket rearranged themselves to minimize the exposure to the solvent. In the crystal structure, F97 and F146 were separated from each other to provide space for chlorobiphenyl group (Fig. 4a). After removal of the ligand, these residues came closer to each other to stabilize the structure, and protein–ligand interactions were replaced by protein–protein intra-molecular interactions. The dimethylamino group of the ligand was in between the h2 and h8 helices (Figs. 1a and 4b). Removal of the ligand allowed reorientations of the E96, L194 and Y195 residues to provide more compact packing (Fig. 4b). It was observed that the h2 helix became shorter (as some of the residues lost the secondary structure), which was maintained throughout the course of the simulation (Fig. S3). Additionally, in the absence of ligand, the S25, Q26 and F27 residues tried to form a helical segment that was a part of an unstructured loop in the presence of ABT737(Fig. S3). Similar kind of observations were also reported in Bcl-xl + Bim binding by Lama et al. in 2013 [34]. Rearrangements of the side-chains in the apo-state caused a drastic change in the landscape of the pocket, making the surface relatively smoother by filling up the cavities and grooves. The P2 pocket became relatively flat (Fig. 4c and d) due to its hydrophobic character (being surrounded by F105, L108, F146, A149, etc.), which did not allow water molecule to enter and occupy the empty space in the absence of ligand.

3.1.2. Bcl-xl complexed with ABT737

The ABT737 inhibitor binds primarily to the P2 and P4 pockets of Bcl-xl. The chlorobiphenyl ring of ABT737 is deeply anchored into the P2 pocket; nitrophenyl sulfonyl benzamide (SO_2 ($PhNO_2$) NH) and the thiophenyl (SPh) ring sit together in the P4 pocket. During MD, the overall binding mode did not deviate from the crystal structure. Binding free energy averaged over the trajectories for ABT737 was −25.2 kcal/mol (Table 1 and Supporting information Table S2).

3.1.3. Bcl-xl complexed with ABT263

The steps for preparing the model of the Bcl-xl + ABT263 (referred as Bxl263) complex are outlined in the 'Methods' section. The structural differences between the two drugs are (i) the replacement of a dimethylamino ($N(CH_3)_2$) group by a morpholino group, (ii) the unsaturation of a phenyl ring of the 'chlorobiphenyl' group followed by introduction of two methyl substituents at the para position of the chlorobiphenyl group and (iii) the replacement of a nitro (NO_2) group by a trifluoromethyl sulfonyl (SO_2CF_3) group (Fig. 1d and Supporting information S1). The first two changes were at positions of the ligand where their conformations were well-specified due to structural constraints. However, for the replacement of the planar NO_2 by the tetrahedral SO_2CF_3 in the P4 pocket, three distinct possibilities with distinctly different stable orientations (separated by 120°) were generated around the S atom. These three possible orientations of the ligand were modeled, and after minimization of the complexes, two of them converged to a similar conformation (Fig. 2a–e). Thus, during minimization to equilibrate the dynamics, two possible conformations of ABT263 were found that have different structural implications on the binding. In one conformation, the thiophenyl (SPh) ring was inside the P4 binding pocket with SO_2CF_3 (Fig. 2f) throughout the simulation. While in another conformation (after minimization, heating and equilibration), the SPh ring moved out of the pocket (Fig. 2g). As these two conformations of the complex were different with respect to the orientation of SPh, they are hereafter referred to as $Bxl263^{in}$ (SPh inside the P4 pocket) and $Bxl263^{out}$ (SPh outside the P4 pocket), and further details about their dynamics are discussed below.

3.1.4. $Bxl263^{in}$

In $Bxl263^{in}$, the SO_2CF_3 and SPh groups are both accommodated simultaneously into the P4 pocket (Fig. 2f, Movie S1). From the MM-GBSA calculation, the binding free energy was −26.4 kcal/mol (Table 1), which was marginally similar to that of ABT737 (−25.2 kcal/mol), indicating that forcing these two groups

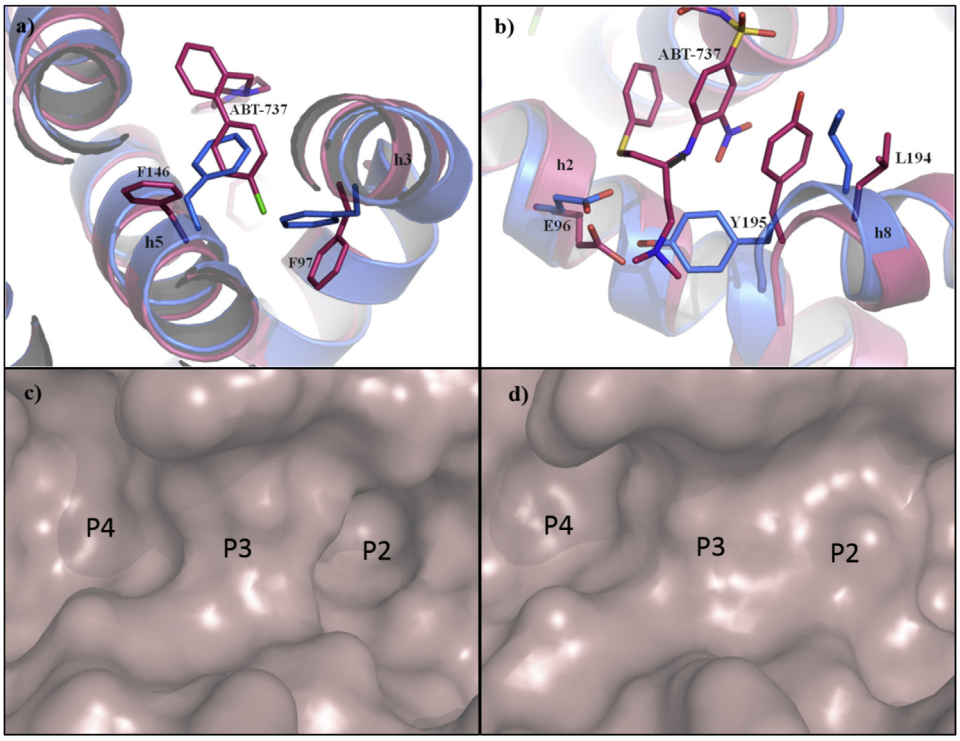

Fig. 4. Superimposed structures of the last snapshots of the simulations of complex (Bxl737, shown in pink color) and uncomplex (Bxl, shown in blue color) states showing the rearrangements of a few residues around the binding pocket. (a) Reorientations of F97 and F146 are observed in P2 after removal of the ligand; (b) reorientations of residues in the h2 and h8 helices (E96, L194 and Y195) were observed in the P4 pocket. Lower panel shows the changes of the landscape of the binding grooves (c) complex and (d) uncomplexed cases. (For interpretation of the references to color in this figure legend, the reader is referred to the web version of this article.)

to remain in P4 together was not very beneficial. Comparisons of the components of the binding energy of ABT263 with ABT737 show that there were gains of 22.7 kcal/mol in van der Waals interactions (certainly due to putting two bulky groups in P4), 6.9 kcal/mol in internal energy and 2.2 kcal/mol in the non-polar component for ABT263. In addition to these gains, there was a loss of 17.4 kcal/mol in total polar interactions (E_{GBEL}). The gain prevailed over the loss and 14.4 kcal/mol gain in total enthalpy were reported (Table 1, Table S2 and Table S3). However, this system suffered a vast entropic penalty ($T\Delta S$), which was 43.6 kcal/mol compared to 30.4 kcal/mol for ABT737 (Table 1). It is exactly what could be expected by keeping two functional groups in the same pocket and restricting their flexibility or conformational freedom.

3.1.5. *Bxl263^{out}*

In Bxl263^{out}, the CF_3 group pointed toward the center of the P4 pocket and pushed the SPh ring toward R100 and Y101 (Fig. S4a), which in turn kicked the SPh out of the pocket (Fig. S4b, Movie S2). This observation was remarkably different from the ABT737 complex. Because ABT737 has an NO_2 group that is smaller in size compared to SO_2CF_3 in ABT263, the nitro group and the SPh ring were both accommodated into the P4 pocket in the Bxl737 complex. For the Bxl263^{out} complex, the SPh did not converge to any stable orientation throughout the 80 ns simulation and remained flexible around the pocket (Fig. 5). The fluctuations of the SPh ring outside the binding pocket were influenced by its interaction with R100 and Y101 of h2 on one side and L194 and Y195 of h8 on another side of the binding pocket (Movie S3). The fluctuations of thiophenyl group is also concerned with the movement of the SO_2CF_3 group within the pocket which is complemented by the Y195 orientations; Y195 orientations create space for these events, as presented in Fig. 5 (also see Supporting information Fig. S7).

The binding free energy of Bxl263^{out} was −44.8 kcal/mol, which is more promising than Bxl737 (−25.2 kcal/mol) and Bxl263^{in} (−26.4 kcal/mol) (Table 1). The components of the MM-GBSA calculations reveal that the placement of the SPh outside the binding pocket results in a drastic loss of the van der Waals stabilization of the complex. In Bxl263^{out}, this component was found to be −70.3 kcal/mol, and a loss of ∼8 kcal/mol was observed compared to Bxl737 in which SPh was comfortably situated in the P4 pocket (Fig. 1c) along with NO_2. It suffered a loss of 30.8 kcal/mol when compared to Bxl263^{in}. The extra van der Waals stabilization was achieved by bringing the two bulkier groups together in P4, but at the cost of other energy components (Table 1, Table S2, Table S3 and Table S4), particularly the entropic penalty. Releasing this strain by a conformational change in SPh loses van der Waals packing, but it immediately improves the benefit from '$E_{internal}$'stress. A gain of 9.4 kcal/mol in $E_{internal}$ was reported. Additionally, the destabilization from polar components ($E_{GB(Polar)+Elec}$) was reduced from 44 kcal/mol to 13.4 kcal/mol, likely because the release of the SPh group from the P4 pocket allows some of the polar residues (R100, Y101, Y195, etc.) to gain access to solvation. The outward movement of the SPh ring increased the flexibility and, thus, there was a gain of 10.4 kcal/mol from the entropic penalty (i.e., +43.6 for the 'in' conformation and + 33.2 kcal/mol for the 'out' conformation: the mentioned values are $T\Delta S$) (Table 1).

3.1.6. *Flipping Y195*

It became difficult for the SPh and SO_2CF_3 groups to coexist with SPh in the P4 binding pocket because there was not enough space in the binding pocket of Bcl-xl. However, Bcl-2 (homolog of Bcl-xl) uses the trick of flipping a tyrosine residue side chain to a completely different orientation (the corresponding dihedral angle is changed) to create space, as observed in the crystal structure (4LVT.PDB) (Fig. S2). This lesson from nature was adopted

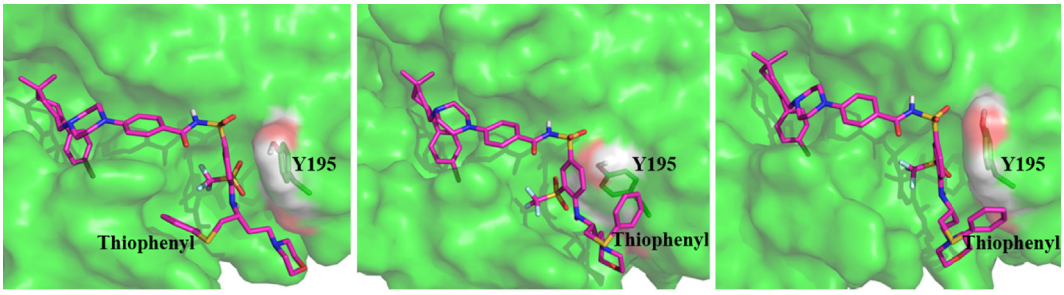

Fig. 5. Snapshots showing the conformations of the ligand (sticks) in the binding pocket of Bcl-xl (green surface) in the Bxl263^{out} trajectory. The orientations of SPh group at different time point and the shift of the position of the SO_2CF_3 group is notable. The orientations of Y195 complements the movements of the ligand. (For interpretation of the references to color in this figure legend, the reader is referred to the web version of this article.)

in the modeling. The side chain conformation of Y195 of Bcl-xl was modeled in two different ways for separate simulations, each with two possible orientations of CF_3 (Fig. 3a and b). The notations Bxl263Y^{rot}cf3-p and Bxl263Y^{rot}cf3-c stands for the two models (to start separate MD runs) having the conformation of side-chain for Y195 the same as in 4LVT, and cf3-p and cf3-c indicate the two different orientations of the CF_3 group. The accessible conformations of Y195 in the structures available in PDBs and in simulations were observed that were found to be distributed in two major clusters (Supporting information Figs. S6 and S7). The enthalpy for Bxl263Y^{rot}cf3-p and Bxl263Y^{rot}cf3-c were −75.3 kcal/mol and −48.8 kcal/mol, respectively (Table 1, Table S8 and Table S9). The ΔGs were −34.9 kcal/mol and −15.6 kcal/mol for Bxl263Y^{rot}cf3-p and Bxl263Y^{rot}cf3-c, respectively (Table 1). Both of the conformations after flipping Y195 showed a reduced affinity compared to Bxl263^{out}, and the leading components for these changes were internal energy and total polar interaction energy ($E_{GB(Polar)+Elec}$). In Bxl263Y^{rot}cf3-c, the SPh ring was kept outside the pocket at the beginning of simulation (similar conformation was observed in Bxl263^{out}, the central orientation of CF_3 removed the ring from the binding pocket) but after ∼5 ns it moved within the pocket. This movement was driven by Y195, R100 and the morpholino group of ligand (Movie S4); the binding affinity suggested that the ligand was not comfortable in this particular arrangement of the surrounding region. Thermodynamic studies suggested that ABT263 has highest binding affinity when the simulation started with the model having the Y195 conformation the same as in 2YXJ, where the SPh ring moved out of the pocket. The interaction energy of Y195 with the ligand was calculated (Supporting information Table S12), and Bxl263^{out} showed maximum stability. It also suggests that the orientation of Y195 with the ligand has a direct effect on the binding affinity. The effect of the change of the pair-wise distance among thiophenyl ring, the trifluoromethyl group and Y195 on the binding affinity was explored. The change in the pair-wise distance over the trajectory for the four different conformations was plotted considering the various orientations of the trifluoromethyl and Y195 (Fig. S5). From the distance-plot, it was found that the distance between CF_3 and SPh in Bxl263Y^{rot}-cf3-c (Fig. S5a) was minimal compared to the other systems when SPh moved inside the pocket. The binding affinity calculated for this system (Bxl263Y^{rot}-cf3-c) was also found to be weaker (Table 1), which confirmed that when the CF_3 and SPh ring came closer, the affinity was reduced. For Bxl263^{out}, this distance was found to be the largest after approximately 12.5 ns of simulation, which facilitated the improvement of the binding affinity. The distances between Y195 and CF_3 and the SPh group were also calculated (Fig. S5b and c). The pair-wise distance between Y195 and CF_3 was minimal for Bxl263^{in} and maximal for Bxl263^{out} (Fig. S5b). The distance between Y195 and the SPh ring was maximal when the thiophenyl ring was outside of the pocket during the initial 5 ns of simulation of Bxl263Y^{rot}-cf3-c. The distance was reduced when the ring moved into the pocket (Fig. S5c) and binding affinity was decreased. It also confirmed that the combined effect of Y195 and these two groups (CF_3 and SPh) of the ligand has a direct influence on the binding.

3.1.7. Modeled Bcl-xl + ABT263 (ModBxl263)

High similarity of Bcl-xl with Bcl-2 and availability of the structure of Bcl-2 with ABT263 gave the opportunity to model the Bcl-xl using Bcl2 + 263 complex as template. Modeling and simulation of the Bcl-xl + 263 (ModBxl263) has shown that in the modeled structure, the SO_2CF_3 and SPh both group remain within the binding pocket while the morpholino group moved away from the protein surface (Fig. 6 and Movie S8). The interaction with the Y195 displaces the morpholino group from its original position, although —SPh and SO_2CF_3 remains anchored into the binding pocket.

The binding free energy was −43.3 kcal/mol, and was comparable with the Bxl263^{out} (Table 1). The fluctuations of the morpholino group compared with Bcl2 + ABT263 under the influence of the orientation of surrounding residues including Y195.

3.1.8. Bcl2 + 263 complex (Bcl263)

The simulation of Bcl2 + 263 in presence of explicit water has also shown that when thiophenyl and —SO_2CF_3 goup both remain inside the binding pocket the morpholino group start moving away from the protein surface (Fig. 7 and Movie S9), which is similar to the microstates of the Bcl-xl complex that was based on this Bcl2 template. From two different tests it has been validated that in a dynamic situation out of these three groups (—SPh, SO_2CF_3 and morpholino) two of them are comfortably anchored and the 3rd is weekly associated. The binding free energy of the modeled Bclxl complex having the morpholino group 'out' doesn't seem to be promising although that should not be a criteria to eliminate the possibility for such a system, all these microstates could coexist (but in different proportion) in a real situation.

3.2. Modification of the ligand: Exploring the alternatives of the SPh group

The dynamic behavior of the structures, as described in previous sections, leads to the interim conclusion that the two groups SO_2CF_3 and —SPh are offering mutually exclusive interactions in a majority of the microstates. In addition to this depending on the orientation of the Y195 (of Bcl-xl) the morpholino group could be weakly associating with the protein surface. These

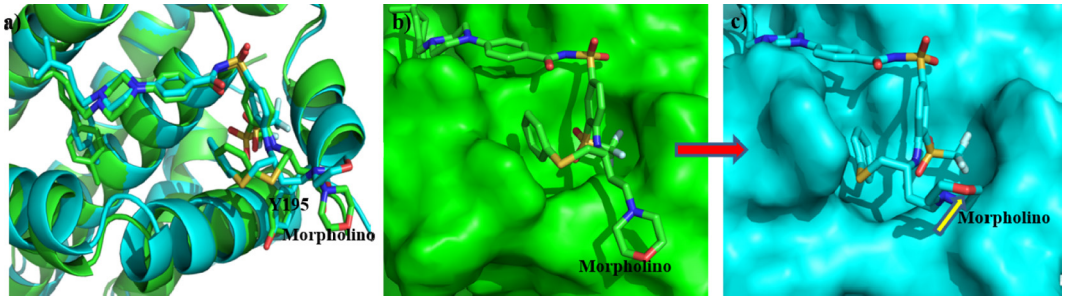

Fig. 6. (a) Superimposed structures of the initial (green) model and the last frame of the simulation of ModBxl263 (cyan), the difference in the positions of the morpholino group is noticeable; the (b) initial and (b) final conformations have been further presented with surface representation of Bcl-xl, using the same color code. (For interpretation of the references to color in this figure legend, the reader is referred to the web version of this article.)

observations raise the question whether a suitably modified ligand can either offer a reduced molecular weight with similar efficacy or can improve the binding affinity further. To get some insight, the —SPh group was tested for some possible modifications. Out of the three groups, only SPh was chosen for modifications because the effect of substitutions of this group was not mentioned in earlier report, whereas two other groups were already claimed to be essential for the drug-like properties (absorption and efficacy) of the ligand [68]. The study suggested auxophoric behavior of the SPh ring that came out of the P4 binding pocket, and it did not converge to any stable conformation (Movie S2). Therefore, this led to a preliminary conclusion that it could be either (i) detached to see whether it was not essential in ABT263, which likely was not checked during the ABT737 → ABT263 transition [68], or (ii) modified further to rescue it from an underutilized situation so that the overall binding affinity of the ligand can be improved further. To investigate these possibilities, several substitutions were attempted, as mentioned below.

3.2.1. *Bcl-xl + ABT263H (Bxl263H)*

The SPh ring was replaced with a hydrogen atom, to switch-off the collisions of a bulky group with the surrounding and the molecule was named ABT263H. Separate simulations for the uncomplexed (ABT263H) and complexed (Bxl263H) states were performed. The binding free energy was found to be −16.4 kcal/mol, and its affinity was lower than Bxl263^{out}. Removal of the SPh ring was predicted to show a loss in van der Waals interactions, but the exact reverse observation was reported from the thermodynamic s calculations. There was a gain of 13.2 kcal/mol in van der Waals interactions and a large loss (∼40 kcal/mol) in total polar contributions ($E_{GB(Polar)+Elec}$) (Table 1 and Table S5). Therefore, this reflects that while the SPh group is flanking outside the pocket (Bxl263^{out}), its van der Walls impact was actually detrimental to the binding. Nevertheless, it had indirect effects to enhance the internal interactions. The loosening of packing could also release some of the restrictions in the bond angles, (dihedral, torsion, etc.), which individually may not be significant but collectively cause a loss of their overall stabilization.

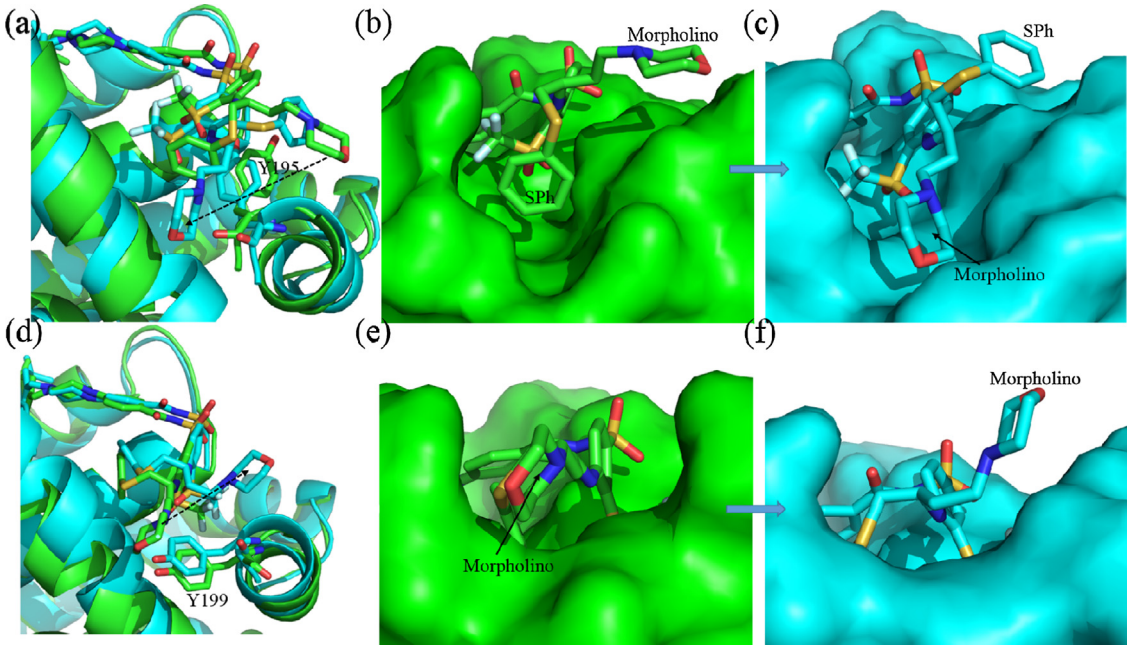

Fig. 7. (a) The superimposed first (green) and last (cyan) frames of the Bxl263^{out} simulations showing the position of Y195; the —SPh group moves out of the pocket, stabilizing the morpholino finally into the binding pocket. The same event has been shown in surface representation of the Bcl-xl with the color codes (b) first (green) (c) last (cyan). The figure (d)–(f) refers to the similar events for Bcl263 simulations, showing the superimposed first and last frames in (d) and the same with surface representations of Bcl-xl in (e) and (f); the color code is same as before. (For interpretation of the references to color in this figure legend, the reader is referred to the web version of this article.)

Table 2
Change in the enthalpy of binding due to the inclusion of interfacial water.

Energy components	Bxl737	Bxl263^{in}	Bxl263^{out}	Bxl263H	Bxl263OH	Bxl263SPhOH	ModBxl263	Bcl2-263
$\Delta\Delta E_{ELEC}$	−6.7	−4.6	−7.7	−50.9	−63.6	−13.6	−8.8	−10.1
$\Delta\Delta E_{VDW}$	−4.5	−1.5	−5.2	−1.7	2	−4	−4.9	−3.7
$\Delta\Delta E_{INTER}$	0.0	0.0	0.0	0.0	−0.2	0.0	0.0	0.0
$\Delta\Delta E_{GB(Polar)}$	5.4	1.9	7.2	24.9	29.5	8.2	5.7	4.1
$\Delta\Delta E_{GB(Nonpolar)}$	−0.8	−0.3	−0.9	−1.0	−0.7	−0.9	−0.8	−0.7
$\Delta\Delta E_{GB(Polar)+Elec}$	−1.3	−2.8	−0.5	−26.0	−34.1	−5.4	−3.0	−6.0
$\Delta\Delta E_{Tot}$ *	−6.6	−4.5	−6.6	−28.7	−33.0	−10.3	−8.7	−10.4
#Water	10	4	10	14	14	11	11	8

§ $\Delta\Delta E = \Delta E_{\text{with interfacial water explicitly}} - \Delta E_{\text{without explicit water}}$.
* $\Delta\Delta E_{Tot} = \Delta E_{\text{TotMM-GBSA with interfacial water explicitly}} - \Delta E_{\text{TotMM-GBSA without explicit water}}$.
# Water = Number of interfacial water molecules falling within the 3 Å cut-off, averaged over the snapshots considered for calculations.

3.2.2. Bcl-xl + ABT263OH (Bxl263OH)

In another attempt, the SPh ring was replaced with an OH group that is much smaller than SPh in size, but more polar, having the scope of forming H-bond with the protein surface if situation demands. This substitution was performed with the notion that the P4 binding pocket has hydrophilic residues and that the replacement of thiophenyl ring with a polar group might add stabilization. The notion works to some extent, showing a gain of ∼25 kcal/mol in total polar contributions (Table 2 and Table S5) compared to the same for Bxl263H. This gain was accompanied by a gain of 3 kcal/mol of internal energy, but there was also an increase of 4.1 kcal/mol in the entropic penalty (TΔS), remaining comparable with Bxl737. Overall, an ∼−22 kcal/mol gain in binding free energy was observed (Table 1, Table S5 and Table S6), and it appeared to be more promising than ABT737, but with a slightly reduced molecular weight. The added —OH group forms a hydrogen bond with R100 (Supporting information Fig. S8). When the energy was compared to Bxl263^{out}, there was a shortage of 6 kcal/mol in binding free energy. The newly formed H-bond was unable to restore the loss in total polar interactions ($E_{GB(Polar+Elec)}$) (Table 1).

3.2.3. Bcl-xl + ABT263SPhOH (Bxl263SPhOH)

The two tests mentioned above that substituted SPh suggested that although the SPh group interacted with the protein non-specifically, it still had some indirect effect on the stabilization of the complex as a consequence of a many-body effect. Therefore, the next attempt was made to modify this group in a manner that can be more associative on the surface of the receptor (without putting it into P4, as that is also destabilizing) and to incorporate new H-bond interactions as a possible strategy. To facilitate this, an OH group was added at the 'para' position of SPh, and the system was named Bxl263SPhOH. The addition of —OH makes the group polar, opening the scope for forming H-bond with the surrounding if the situation demands. The obtained binding free energy was −56.3 kcal/mol (Table 1 and Table S7), which reflects a stronger association of the ligand and receptor compared to Bxl263^{out} (Table 1). Movie S5 shows that SPhOH was more associative on the surface of the complex, and thus, it brought some extra stabilization to the binding. Although it is still unable to become optimized to any specific conformation, it nevertheless spent more time on the protein surface compared to SPh in Bxl263^{out} (Movie S2 and S5). The SPh in Bxl263^{out} flanks outside the pocket, projecting itself away from the surface (Movie S2). The major gain in binding came from the van der Waals ($\Delta\Delta E_{vdw} \sim 14$ kcal/mol) and internal energy ($\Delta\Delta E_{internal}$ 10.7 kcal/mol) (here the notation 'ΔΔE' indicates the difference between ABT263^{out} and ABT263SPhOH for a specific component of binding energy). Although there was penalty of 13.2 kcal/mol in the total polar interactions ($\Delta\Delta E_{GB+Elec}$), this loss was overcome by the gain in van der Waals and internal energy components, and an overall gain of 12.6 kcal/mol was observed in enthalpy ($\Delta\Delta E_{MM(Total)}$), which was reflected in the binding free energy (Table 1, Tables S4 and S7). Although it can apparently be argued that the attachment of a polar group (OH) should enhance the polar interactions in the binding process, it did the opposite in practice. This has likely been the case because the formation of the polar interactions between SPhOH and the protein surface make more complex changes that are distributed over multiple atoms, bonds, angles, and dihedrals whose collective changes are reflected in the van der Waals and internal energy components. Additionally, the increase in the polar character of the ligand comes with a larger penalty of desolvation upon complexation, and thus, the sum of GB(Polar) and electrostatics showed more penalties for this system than Bxl263^{out}. The resultant effect overcame the negative impact on the sum of the change in coulomb interactions. This is a good example of indirect interactions, where the perturbation in one type of interaction gets amplified and impacts all possible interactions in the surrounding region in a correlated manner.

3.2.4. Role of explicit water in the binding free energy calculations

The inspection of the simulated snapshots of the different systems revealed that often the interactions between the ligands and the receptors are mediated by water molecules (Fig. 8). Even in the crystal structure of ABT737 with Bcl-xl, it was observed that there were 98 molecules of crystal water present; among them, some of the water molecules were found to be strategically placed between the ligand and the receptor to facilitate interactions (Supporting information Fig. S9). Because the crystallographic data do not contain the position of the H-atoms, their role in bridging the interactions between the ligand and the protein through H-bond was unclear. The importance of the water in biological molecules is known to be important [53,69,70]. The clues from the dynamics and crystal structure gave us the motivation to carefully investigate the atomistic details of the interactions (receptor–ligand) (Fig. 8 and Supporting information Fig. S9) in presence of explicit water molecules in the simulated conformations. The inclusion of the important explicit water molecules in the MM-GBSA calculations is not always straightforward, and the results are sensitive to the criteria of identifying the water molecules. Recently, Zhu et al. used an intermediate approach by considering the explicit water molecules within approximately 3.5 Å of the protein and ligand and performed the MM-PBSA [65]. This strategy of selecting important water does not have many mathematical foundations, but it has shown good correlation with the experimental data. In the present report, the MM-GBSA calculations were repeated after inclusion of the water molecules within 3 Å from both the protein and the ligand (the details of the strategy have been provided in the Methods section). The shifts in the binding enthalpy ($\Delta\Delta E_{Tot} = \Delta\Delta E_{mm} + \Delta\Delta E_{solvation}$) from the 'implicit-only' MM-GBSA calculations are listed in Table 4. The results showed that the magnitudes of $\Delta\Delta E_{Tot}$ were correlated with the number of interfacial waters that were selected for each system with the same criteria. For Bxl737, there were

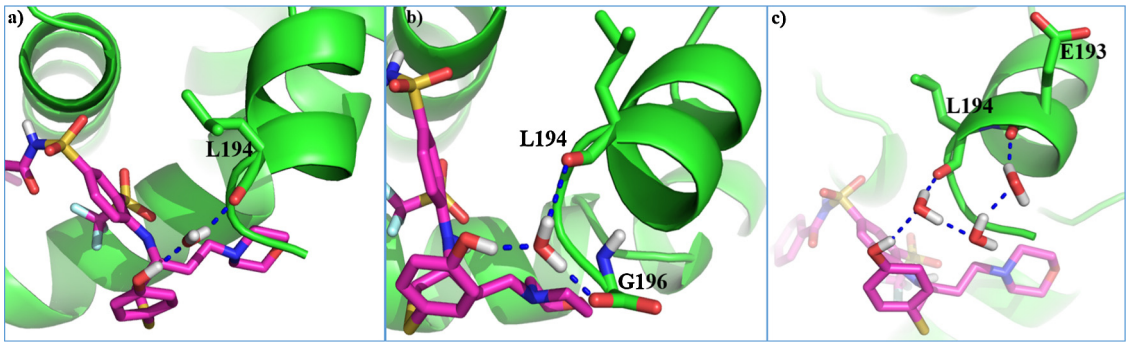

Fig. 8. Representative snapshots showing the interactions of ligand with Bcl-xl mediated by the 'bridging water' molecules in the complex Bxl263SPhOH.

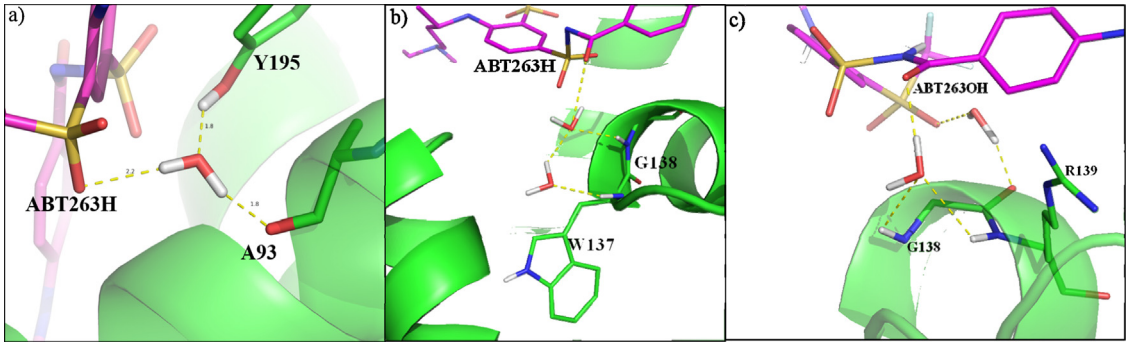

Fig. 9. Representative snapshots showing the water mediated interactions in (a) ABT263H, (b) ABT263H and (c) ABT263OH with Bcl-xl.

10 selected explicit water molecules, and the change in enthalpy ($\Delta\Delta E_{Tot}$) was −6.6 kcal/mol (Table 2). In the case of Bxl263^{in}, where the larger SO_2CF_3 and SPh are both inside the P4 binding pocket, the number of interfacial water molecules was much less (only 4), and that led to a −4.5 kcal/mol gain ($\Delta\Delta E_{Tot}$) in the enthalpy. In Bxl263^{out}, the outward movement of the SPh ring created space in the P4 binding pocket that resulted in an increase in the number of interfacial water molecules, and the change in enthalpy was −6.6 kcal/mol. Surprising results were found for Bxl263H and Bxl263OH, where 14 interfacial water molecules were selected and were associated with a larger gain in enthalpy (−28.7 kcal/mol for Bxl263H and −33.0 kcal/mol in Bxl263OH) (Table 2). The inspection of the structures obtained from the simulations of Bxl263^{out}, Bxl263H and Bxl263OH revealed that in Bxl263^{out}, the SPh ring was behaving like an umbrella and preventing the entry of a few water molecules, which is reflected in the number of interfacial water molecules (Fig. S10). In the case of Bxl263H, one static water molecule was observed throughout the simulation, which was trapped by hydrogen bonds with the ligand through Y195 and A93 (Fig. 9a, Movie S6). Another water molecule also mediated the interactions of W137 and G138 with the ligand through hydrogen bonds (Fig. 9b). In Bxl263OH, two hydrogen bonds between the ligand and the water molecules were maintained throughout the trajectory (Movie S7), although the identity of the water molecules changed dynamically such that one molecule was continuously replaced by another. The interfacial water in Bxl263OH also acted like a bridge and connected G138 and R139 with ligand by H-bonds (Fig. 9c), which led to further stabilization of the interactions (Table 2). In Bxl263SPhOH, eleven interfacial water molecules were selected (averaged over time), and the change in enthalpy was −10.3 kcal/mol. An alternative view of the interactions, including the bridging water has been provided in the Supporting information (Fig. S11), prepared by ligplot [38].

4. Discussion

The objective of the study was to investigate the molecular level interactions between ABT263 and Bcl-xl and to understand the similarities and dissimilarities with that of ABT737. The experimentally determined structure of the Bxl737 complex (2YXJ) and Bcl2-263 (4LVT) were the starting templates. As described in the results, multiple starting structures for separate simulations were modeled by considering all possible stable conformations of several functional groups and amino acid side chains. All of them were simulated separately, and the binding free energies were calculated, which gave a relative estimation of the preference for a particular conformation. The newly added functional groups that were substituted on ABT737 had multiple possible rotamers, and the Y195 side-chain could also had possible multiple conformations. All of the combinations were modeled, but after energy minimization and short simulations, a few starting conformations converged to similar orientations (Fig. 2). The binding free energy calculations showed that the central orientation of CF_3 and outward orientation of the SPh ring (Bxl263^{out}) was the most preferred combination for the complexation with ABT263. The structure of the homologous Bcl2 complexed with ABT263 suggested that Y195 could adapt an orientation that was different from the Bxl737 complex. Another conformation of Bxl263 (ModBcl-xl + ABT263) was modeled using 4LVT as a template. Simulation has shown that the morpholino group start moving away from the protein surface (Fig. 6 and Movie S8). The same effect is also evident in the complex of the Bcl-2 + ABT263 (4LVT) whose simulation has demonstrated that the morpholino group of the ABT263 moved away from the surface of protein (Fig. 7), revealing a departure from the crystallographic conformation in a solvated condition. So the interference of the Y195 (and Y199 for the case of Bcl2) with the ligand is evident from the simulations. The possible mechanism of eliminations of these interactions in the microstates was tested by modeling the

tyrosine orientations in different ways. To complement this, two different orientations of the CF_3 group were tested (Bxl263Y^{rot}cf3-c and Bxl263Y^{rot}cf3-p) (Fig. 3). In contrast to the previous orientation of Y195 (as reported in 2YXJ), these combinations of altered orientations of Y195 and $-CF_3$ allowed the thiophenyl ring to remain inside the pocket. In Bxl263Y^{rot}cf3-c, the SPh ring was initially kept outside of the pocket as it was in Bxl263^{out}, where the central orientation of CF_3 kicked out the SPh ring. However, within 5 ns of simulation, the ring moved inside the pocket due to the interactions with Y195 and R100 (Movie S4). Here, simulation showed that Y195 and R100 pushed the SPh ring into the pocket, but this conformation had a reduced affinity compared to Bxl263^{out} (Table 1). Meanwhile, in Bxl263Y^{rot}cf3-p, the SPh ring remained within the pocket throughout the simulation, similar to Bxl263^{in}. The binding energy results suggested that, among the various conformations, the microstates of Bxl263^{out} are the preferred conformations for the complex. The relationship between changes in binding affinity and changes in the orientations of the SPh ring, the CF_3 group and Y195 underscored the significance of these groups on ligand binding. The pair-wise distance between these three groups was plotted for four systems in Fig. S5. The interaction energy of Y195 with ligand was maximal for Bxl263^{out} (Table S12). A comparison of the stability of different binding conformations suggested that Bxl263^{out} was the most favorable conformation because the thiophenyl ring flanks the binding pocket (Fig. 2g), which raised the question of whether the thiophenyl ring was essential for the binding. To examine this, the ring was deleted (i.e., substituted by 'H' atom), but it reduced the binding affinity. This implies that although the thiophenyl ring did not directly interact with the binding pocket, it had indirect complex effects whose presence were felt by the region surrounding it, e.g., the effect of its dynamics could propagate to the nearby residues even through solvent. With this lesson, a hydroxyl group was attached to thiophenyl ring to preserve the SPh group on the ligand and, at the same time, to bring it close to the surface of protein through polar interactions without placing it into the binding pocket. Indeed, this strategy improved the binding free energy, and it was often observed that the OH group required the help of water molecules to bridge the interactions with the protein surface (Fig. 8). The presence of a hydrophilic residue around the P4 pocket also indicated that water could help at this site to form favorable interactions between the ligand and receptor. The role of water in mediating the interactions among molecules is very well known and has been reported in the literature [52,53,65,69,71–73]. The standard MM-GBSA calculation treats the solvent as a continuous medium and thus ignores the effect of explicit atomic descriptions of the polar interactions between the macromolecules and the solvent. To include the effect of some critical water molecules in the binding energy, a second set of MM-GBSA calculations was performed after selecting the water molecules within 3 Å from both the ligand and the receptor. The difference in results obtained with and without these explicit water molecules is denoted by $\Delta\Delta E_{Tot}$ and is listed in Table 2. Interesting results were observed for the ligands where the thiophenyl ring was replaced with hydrogen and hydroxyl groups, as the change in enthalpy was much larger compared to other substitutions. Interfacial water counts suggested that removal of the thiophenyl ring allowed the entry of extra water molecules, whose effect was reflected in binding enthalpy. From structural analysis, it was found that the hydrophobic phenyl ring behaved like an umbrella and prevented the entry of the water molecule, and its deletion allowed the entry of those water molecules in the P4 pocket. The number of water molecules was nicely correlated with the change in enthalpy (Table 2). This clearly suggests that water molecules play an essential role for binding in the hydrophilic pocket. The inclusion of such constitutional water is also critical to get a true estimate of the van der Waals packing between the ligand and the receptor. If the water molecules, which were used explicitly during the simulation, are removed prior to MM-GBSA calculation, it would create a vacuum at the protein–ligand interface, and important interactions could be missed. This might reflect a weaker van der Waals packing due to the creation of the vacuum that does not mimic the actual event in most cases. This type of situation has been confirmed by the difference in van der Waals interactions created by interfacial water as listed in Table 2. The most sensitive systems with respect to van der Waals interactions are Bxl263^{out}, Bxl263SPhOH and ModBxl263 as they have flanking groups and thus can have water molecules take part in the packing. The substitution of the bulky SPh group by an 'H' atom of negligible volume or by the much smaller OH group have a binding affinity that is very sensitive to the consideration of constitutional water. This is because the deletion of such a bulky group makes a wide region on the protein and ligand surface exposed to the solvent, and thus, the polar interaction network gets reshuffled during the simulation in presence of explicit water (Table 2).

The limitation of the results presented here is that they cannot directly confirm whether the MM-GBSA data, including the explicit water molecules, would be more acceptable than the same calculations that exclude it. This is primarily because of the lack of sufficient experimental thermodynamic measurements on ABT737 and ABT263 to date and also because MM-GBSA is more reliable for relative ordering rather than trusting the absolute values of the computed free energies. It might be argued that the magnitude of the computed binding free energy is high and very different from the standard range of experimentally determined values of binding free energy of the ligands (usually ~10 kcal/mol). The arguments based on the closeness to the experimental data are not always meaningful. This deviation is due to the limitation of the MM-GBSA protocol, which has a dependency on the force-field, and the limitation of the parameterization of the small molecule. This is why the absolute values may differ from one parameter set to another, although, ideally they are supposed to preserve the trend. Nevertheless, the MM-GBSA method is well accepted as a standard tool to rank the ligands relative to each other when comparing the absolute values with the experimentally determined free energies [74].

Often MM-PBSA is advocated as being a more acceptable method than MM-GBSA for this type of free energy-based comparison. However, as discussed in Section 2, the particular type of GB method, such as the GBMV method used in this work, has already been benchmarked to have a strong correlation with the MM-PBSA calculation [62]. The use of GBMV in this MM-GBSA calculation provides an advantage of computing speed over MM-PBSA that enabled the averaging of data over a huge number of snapshots, enhancing the quality of the 'statistics' involved in the data.

For this present system, although the consideration of the explicit water (comparing Tables 1 and 2) preserves the relative order of the ABT737 and the conformations of ABT263, it elucidates ABT263OH as a promising substitution and comparable with ABT263. The arguments can be made in support of the higher reliability of the data in that it has shown very good correlation of the selected number of explicit water molecules with the energy change (Table 2: $\Delta\Delta E_{Tot}$). Furthermore, it can clearly account for the strong effect of the bridging water molecules compared to the implicit and average effect, which are often the discriminating factor between two ligands. Moreover, Table 2 clearly shows that it also impacted the van der Waals term, whose reason and implication has been explained in the results section. The inclusion of structural water molecules is an increasingly preferred protocol in molecular modeling [75,76].

5. Conclusions

The mechanism of ABT263 binding to inhibit Bcl-xl was investigated. A model of the complex was constructed based on the

available structure of ABT737 with Bcl-xl and ABT263 with Bcl2. The relaxation of the Bxl263 complex using MD simulation gave us an advantage to witness the critical departure from its starting conformation to optimize an alternate binding mode, clearly elucidating the salient features that are unique for ABT263 binding. The early stages of modeling and short MD simulations revealed that the functional groups of the ligand interfere with each other. Nevertheless, ABT263 is capable of overcoming the loss, as the resultant effect of all of the changes it has compared to ABT737. The conformations sampled by the windows of separate trajectories of individual systems grossly suggest that the most favored microstates have either with —SPh or the morpholino anchored into binding pocket of Bcl-xl, not simultaneously. The orientations of the Y195 have the capability to modulate this. In true sense the free energy shall be a reflection of the mixture of all possible conformational microstates in different ratios, whose measurement is beyond the scope of available methods. Within the limited scope of the study, the computed free energies of these two subspaces indicate that their population might be competing. Suitable modification of either group can shift the equilibrium to be dominated by one conformation, along with possible enhancement in binding affinity. Since the role of morpholino group has already been reported to determine the drug-like properties, it was not considered modification and so only the SPh substitutions were tested. Simulations revealed that the addition of an OH group on —SPh improved the binding affinity. This series of computational tests also suggested that, in hydrophilic binding pocket, water could bridge many interactions and played crucial roles in the binding affinity. For example, the OH group that was grafted on SPh formed this type of interactions utilizing water. However, this structural insight would be missed if the computation of binding free energy did not include such constitutional water molecules explicitly. Inclusion of constitutional water explicitly in the free energy calculation protocol elucidated ABT263OH as a promising lead compound. Overall, the computed free energy and the mechanistic insights have highlighted the scope to improve the efficiency of the ligands against Bcl-xl at least in principle and certainly provide the motivation for *in-vitro* tests in future studies.

Acknowledgements

The work is funded by the project no. BT/PR793/BID/7/370/2011 sanctioned by the Department of Biotechnology (DBT), Government of India. PP receives funding from UGC (Government of India). AM receives funding from CSIR (Government of India), and SM is funded by the CoE program of DBT (Government of India) running at the Bioinformatics Center, Bose Institute.

Appendix A. Supplementary data

Supplementary data associated with this article can be found, in the online version, at http://dx.doi.org/10.1016/j.jmgm.2015.02.005.

References

[1] J.F. Kerr, A.H. Wyllie, A.R. Currie, Apoptosis: a basic biological phenomenon with wide-ranging implications in tissue kinetics, Br. J. Cancer 26 (1972) 239–257.
[2] M.O. Hengartner, The biochemistry of apoptosis, Nature 407 (2000) 770–776.
[3] H. Harada, S. Grant, Apoptosis regulators, Rev. Clin. Exp. Hematol. 7 (2003) 117–138.
[4] S. Fulda, K.M. Debatin, Extrinsic versus intrinsic apoptosis pathways in anticancer chemotherapy, Oncogene 25 (2006) 4798–4811.
[5] G.V. Putcha, C.A. Harris, K.L. Moulder, R.M. Easton, C.B. Thompson, E.M. Johnson Jr., Intrinsic and extrinsic pathway signaling during neuronal apoptosis: lessons from the analysis of mutant mice, J. Cell Biol. 157 (2002) 441–453.
[6] J.M. Adams, S. Cory, The Bcl-2 protein family: arbiters of cell survival, Science 281 (1998) 1322–1326.
[7] D.T. Chao, S.J. Korsmeyer, BCL-2 family: regulators of cell death, Annu. Rev. Immunol. 16 (1998) 395–419.
[8] S. Cory, J.M. Adams, The Bcl2 family: regulators of the cellular life-or-death switch, Nat. Rev. Cancer 2 (2002) 647–656.
[9] J.C. Martinou, D.R. Green, Breaking the mitochondrial barrier, Nat. Rev. Mol. Cell Biol. 2 (2001) 63–67.
[10] C. Adrain, S.J. Martin, The mitochondrial apoptosome: a killer unleashed by the cytochrome seas, Trends Biochem. Sci. 26 (2001) 390–397.
[11] C. Borner, The Bcl-2 protein family: sensors and checkpoints for life-or-death decisions, Mol. Immunol. 39 (2003) 615–647.
[12] J.M. Adams, S. Cory, Life-or-death decisions by the Bcl-2 protein family, Trends Biochem. Sci. 26 (2001) 61–66.
[13] A. Maity, S. Yadav, C.S. Verma, S. Ghosh Dastidar, Dynamics of Bcl-xL in water and membrane: molecular simulations, PLoS ONE 8 (2013) e76837.
[14] J.C. Reed, H. Zha, C. Aime-Sempe, S. Takayama, H.G. Wang, Structure-function analysis of Bcl-2 family proteins. Regulators of programmed cell death, Adv. Exp. Med. Biol. 406 (1996) 99–112.
[15] S. Kharbanda, P. Pandey, L. Schofield, S. Israels, R. Roncinske, K. Yoshida, et al., Role for Bcl-xL as an inhibitor of cytosolic cytochrome C accumulation in DNA damage-induced apoptosis, Proc. Natl. Acad. Sci. U.S.A. 94 (1997) 6939–6942.
[16] S.H. Leech, R.A. Olie, O. Gautschi, A.P. Simoes-Wust, S. Tschopp, R. Haner, et al., Induction of apoptosis in lung-cancer cells following bcl-xL anti-sense treatment, Int. J. Cancer 86 (2000) 570–576.
[17] I. Lebedeva, R. Rando, J. Ojwang, P. Cossum, C.A. Stein, Bcl-xL in prostate cancer cells: effects of overexpression and down-regulation on chemosensitivity, Cancer Res. 60 (2000) 6052–6060.
[18] A.P. Simoes-Wust, R.A. Olie, O. Gautschi, S.H. Leech, R. Haner, J. Hall, et al., Bcl-xl antisense treatment induces apoptosis in breast carcinoma cells, Int J Cancer (Journal International du Cancer) 87 (2000) 582–590.
[19] H. Friess, Z. Lu, A. Andren-Sandberg, P. Berberat, A. Zimmermann, G. Adler, et al., Moderate activation of the apoptosis inhibitor bcl-xL worsens the prognosis in pancreatic cancer, Ann Surg 228 (1998) 780–787.
[20] G.L. Verdine, L.D. Walensky, The challenge of drugging undruggable targets in cancer: lessons learned from targeting BCL-2 family members, Clin. Cancer Res. 13 (2007) 7264–7270.
[21] A. Maity, S. Majumdar, P. Priya, P. De, S. Saha, S. Ghosh Dastidar, Adaptability in protein structures: structural dynamics and implications in ligand design, J. Biomol. Struct. Dyn. 33 (2) (2014) 298–321.
[22] N. Bharatham, S.W. Chi, H.S. Yoon, Molecular basis of Bcl-X(L)-p53 interaction: insights from molecular dynamics simulations, PLoS ONE 6 (2011) e26014.
[23] J.C. Reed, Mechanisms of apoptosis, Am. J. Pathol. 157 (2000) 1415–1430.
[24] P.E. Czabotar, E.F. Lee, M.F. van Delft, C.L. Day, B.J. Smith, D.C. Huang, et al., Structural insights into the degradation of Mcl-1 induced by BH3 domains, Proc. Natl. Acad. Sci. U.S.A. 104 (2007) 6217–6222.
[25] A.M. Petros, E.T. Olejniczak, S.W. Fesik, Structural biology of the Bcl-2 family of proteins, BBA-Mol. Cell Res. 1644 (2004) 83–94.
[26] P.J. Hajduk, SAR by NMR: putting the pieces together, Mol. Interv. 6 (2006) 266–272.
[27] E.F. Lee, P.E. Czabotar, B.J. Smith, K. Deshayes, K. Zobel, P.M. Colman, et al., Crystal structure of ABT-737 complexed with Bcl-xL: implications for selectivity of antagonists of the Bcl-2 family, Cell Death Differ. 14 (2007) 1711–1713.
[28] T. Oltersdorf, S.W. Elmore, A.R. Shoemaker, R.C. Armstrong, D.J. Augeri, B.A. Belli, et al., An inhibitor of Bcl-2 family proteins induces regression of solid tumours, Nature 435 (2005) 677–681.
[29] C. Tse, A.R. Shoemaker, J. Adickes, M.G. Anderson, J. Chen, S. Jin, et al., ABT-263: a potent and orally bioavailable Bcl-2 family inhibitor, Cancer Res. 68 (2008) 3421–3428.
[30] M. Konopleva, R. Contractor, T. Tsao, I. Samudio, P.P. Ruvolo, S. Kitada, et al., Mechanisms of apoptosis sensitivity and resistance to the BH3 mimetic ABT-737 in acute myeloid leukemia, Cancer cell 10 (2006) 375–388.
[31] D. Merino, S.L. Khaw, S.P. Glaser, D.J. Anderson, L.D. Belmont, C. Wong, et al., Bcl-2, Bcl-x(L), and Bcl-w are not equivalent targets of ABT-737 and navitoclax (ABT-263) in lymphoid and leukemic cells, Blood 119 (2012) 5807–5816.
[32] D. Lama, R. Sankararamakrishnan, Molecular dynamics simulations of pro-apoptotic BH3 peptide helices in aqueous medium: relationship between helix stability and their binding affinities to the anti-apoptotic protein Bcl-X-L, J. Comput. Aid. Mol. Des. 25 (2011) 413–426.
[33] S. Acoca, Q. Cui, G.C. Shore, E.O. Purisima, Molecular dynamics study of small molecule inhibitors of the Bcl-2 family, Proteins 79 (2011) 2624–2636.
[34] D. Lama, V. Modi, R. Sankararamakrishnan, Behavior of solvent-exposed hydrophobic groove in the anti-apoptotic Bcl-X-L protein: clues for its ability to bind diverse BH3 ligands from MD simulations, PLoS ONE (2013) 8.
[35] A.J. Souers, J.D. Leverson, E.R. Boghaert, S.L. Ackler, N.D. Catron, J. Chen, et al., ABT-199, a potent and selective BCL-2 inhibitor, achieves antitumor activity while sparing platelets, Nat. Med. 19 (2013) 202–208.
[36] Accelrys Software Inc., Discovery Studio Modeling Environment, Release 3.5, Accelrys Software Inc., San Diego, CA, 2012.
[37] B.K. Kuntal, P. Aparoy, P. Reddanna, EasyModeller:, A graphical interface to MODELLER, BMC Res. Notes 3 (2010) 226.
[38] R.A. Laskowski, M.B. Swindells, LigPlot+: multiple ligand-protein interaction diagrams for drug discovery, J. Chem. Inf. Model. 51 (2011) 2778–2786.
[39] S. Jo, T. Kim, V.G. Iyer, W. Im, CHARMM-GUI: a web-based graphical user interface for CHARMM, J. Comput. Chem. 29 (2008) 1859–1865.

[40] W.L. Jorgensen, J. Chandrasekhar, J.D. Madura, R.W. Impey, M.L. Klein, Comparison of simple potential functions for simulating liquid water, J. Chem. Phys. 79 (1983) 926–935.
[41] J.C. Phillips, R. Braun, W. Wang, J. Gumbart, E. Tajkhorshid, E. Villa, et al., Scalable molecular dynamics with NAMD, J. Comput. Chem. 26 (2005) 1781–1802.
[42] A. Mackerell, M. Feig, C. Brooks, Extending the treatment of backbone energetics in protein force fields: limitations of gas-phase quantum mechanics in reproducing protein conformational distributions in molecular dynamics simulations, J. Comput. Chem. 25 (2004) 1400.
[43] A.D. MacKerell Jr., M. Feig, C.L. Brooks III, Improved treatment of the protein backbone in empirical force fields, J. Am. Chem. Soc. 126 (2004) 698–699.
[44] K. Vanommeslaeghe, A.D. MacKerell Jr., Automation of the CHARMM General Force Field (CGenFF) I: Bond perception and atom typing, J. Chem. Inf. Model 52 (2012) 3144–3154.
[45] T. Darden, L. Perera, L. Li, L. Pedersen, New tricks for modelers from the crystallography toolkit: the particle mesh Ewald algorithm and its use in nucleic acid simulations, Structure 7 (1999) R55–R60.
[46] W. Humphrey, A. Dalke, K. Schulten, VMD: visual molecular dynamics, J. Mol. Graph. 14 (1996) 27–28, 33-8.
[47] W.L. DeLano, The Pymol Molecular Graphics System, DeLano Scientific, San Carlos, CA USA, 2002.
[48] M.K. Gilson, J.A. Given, B.L. Bush, J.A. McCammon, The statistical-thermodynamic basis for computation of binding affinities: a critical review, Biophys. J. 72 (1997) 1047–1069.
[49] J.M. Swanson, R.H. Henchman, J.A. McCammon, Revisiting free energy calculations: a theoretical connection to MM/PBSA and direct calculation of the association free energy, Biophys. J. 86 (2004) 67–74.
[50] Advances in Protein Chemistry and Structural Biology, Computational Chemistry Methods in Structural Biology, In: Christo, C. (Ed.), Academic Press, 2011, vol. 85.
[51] B. Kuhn, P. Gerber, T. Schulz-Gasch, M. Stahl, Validation and use of the MM-PBSA approach for drug discovery, J. Med. Chem. 48 (2005) 4040–4048.
[52] W. Treesuwan, S. Hannongbua, Bridge water mediates nevirapine binding to wild type and Y181C HIV-1 reverse transcriptase—evidence from molecular dynamics simulations and MM-PBSA calculations, J. Mol. Graph. Model. 27 (2009) 921–929.
[53] S. Wong, R.E. Amaro, J.A. McCammon, MM-PBSA captures key role of intercalating water molecules at a protein–protein interface, J. Chem. Theory Comput. 5 (2009) 422–429.
[54] J.M. Hayes, V.T. Skamnaki, G. Archontis, C. Lamprakis, J. Sarrou, N. Bischler, et al., Kinetics, in silico docking, molecular dynamics, and MM-GBSA binding studies on prototype indirubins, KT5720, and staurosporine as phosphorylase kinase ATP-binding site inhibitors: the role of water molecules examined, Proteins 79 (2011) 703–719.
[55] P.D. Lyne, M.L. Lamb, J.C. Saeh, Accurate prediction of the relative potencies of members of a series of kinase inhibitors using molecular docking and MM-GBSA scoring, J. Med. Chem. 49 (2006) 4805–4808.
[56] V. Zoete, M.B. Irving, O. Michielin, MM-GBSA binding free energy decomposition and T cell receptor engineering, J. Mol. Recognit. 23 (2010) 142–152.
[57] G. Rastelli, A. Del Rio, G. Degliesposti, M. Sgobba, Fast and accurate predictions of binding free energies using MM-PBSA and MM-GBSA, J. Comput. Chem. 31 (2010) 797–810.
[58] P.A. Kollman, I. Massova, C. Reyes, B. Kuhn, S. Huo, L. Chong, et al., Calculating structures and free energies of complex molecules: combining molecular mechanics and continuum models, Acc. Chem, Res. 33 (2000) 889–897.
[59] B. Kuhn, P.A. Kollman, Binding of a diverse set of ligands to avidin and streptavidin: an accurate quantitative prediction of their relative affinities by a combination of molecular mechanics and continuum solvent models, J. Med. Chem. 43 (2000) 3786–3791.
[60] A. Onufriev, D.A. Case, D. Bashford, Effective Born radii in the generalized Born approximation: the importance of being perfect, J. Comput. Chem. 23 (2002) 1297–1304.
[61] M.S. Lee, F.R. Salsbury, C.L. Brooks, Novel generalized Born methods, J. Chem. Phys. 116 (2002) 10606–10614.
[62] M.S. Lee, M. Feig, F.R. Salsbury Jr., C.L. Brooks III, New analytic approximation to the standard molecular volume definition and its application to generalized Born calculations, J. Comput. Chem. 24 (2003) 1348–1356.
[63] M. Feig, Modeling Solvent Environments: Applications to Simulations of Biomolecules, John Wiley & Sons, Weinheim, 2009.
[64] S.G. Dastidar, D.P. Lane, C.S. Verma, Multiple peptide conformations give rise to similar binding affinities: molecular simulations of p53-MDM2, J. Am. Chem. Soc. 130 (2008) 13514–13515.
[65] Y.L. Zhu, P. Beroza, D.R. Artis, Including explicit water molecules as part of the protein structure in MM/PBSA calculations, J. Chem. Inf. Model. 54 (2014) 462–469.
[66] P.A. Greenidge, C. Kramer, J.C. Mozziconacci, R.M. Wolf, MM/GBSA binding energy prediction on the PDBbind data set: successes, failures, and directions for further improvement, J. Chem. Inf. Model. 53 (2013) 201–209.
[67] L. Delgado-Soler, M. Pinto, K. Tanaka-Gil, J. Rubio-Martinez, Molecular determinants of Bim(BH3) peptide binding to pro-survival proteins, J. Chem. Inf. Model. 52 (2012) 2107–2118.
[68] M.D. Wendt, Discovery of ABT-263, a Bcl-family protein inhibitor: observations on targeting a large protein–protein interaction, Expert Opin. Drug Discovery 3 (2008) 1123–1143.
[69] J.E. Ladbury, Just add water! The effect of water on the specificity of protein–ligand binding sites and its potential application to drug design, Chem. Biol. 3 (1996) 973–980.
[70] E. Meyer, Internal water molecules and H-bonding in biological macromolecules: a review of structural features with functional implications, Protein Sci. 1 (1992) 1543–1562.
[71] M. Levitt, B.H. Park, Water: now you see it, now you don't, Structure 1 (1993) 223–226.
[72] S. Fischer, C.S. Verma, Binding of buried structural water increases the flexibility of proteins, Proc. Natl. Acad. Sci. U.S.A. 96 (1999) 9613–9615.
[73] Z. Li, T. Lazaridis, Thermodynamics of buried water clusters at a protein–ligand binding interface, J. Phys. Chem. B 110 (2006) 1464–1475.
[74] T. Hou, J. Wang, Y. Li, W. Wang, Assessing the performance of the MM/PBSA and MM/GBSA methods. 1. The accuracy of binding free energy calculations based on molecular dynamics simulations, J. Chem. Inf. Model. 51 (2011) 69–82.
[75] C.S. Poornima, P.M. Dean, Hydration in drug design. 1. Multiple hydrogen-bonding features of water molecules in mediating protein–ligand interactions, J. Comput. Aided Mol. Des. 9 (1995) 500–512.
[76] V. Mikol, C. Papageorgiou, X. Borer, The role of water molecules in the structure-based design of (5-hydroxynorvaline)-2-cyclosporin: synthesis, biological activity, and crystallographic analysis with cyclophilin A, J. Med. Chem. 38 (1995) 3361–3367.